A spray drying system for synthesis of rare-earth doped cerium oxide nanoparticles

Vaneet Sharma[a], Kathryn M. Eberhardt[a], Renu Sharma[a,b,c] James B. Adams[a], and Peter A. Crozier[a]

[a]School of Mechanical, Aerospace, Chemical and Materials Engineering, Arizona State University, Tempe, Arizona 85287-6106
[b]Leroy Eyring Center for Solid State Science, Arizona State University, Tempe, Arizona 85287-9506
[c]Currently at Center for Nanoscale Science and Technology, National Institute of Standards and Technology, Gaithersburg, MD 20899-6203

Abstract

We have constructed a spray-dryer to synthesize doped ceria nanoparticles. The system was employed to synthesize mixed oxide nanoparticles of praseodymium doped CeO_2 ($Ce_{0.97}Pr_{0.03}O_2$, $Ce_{0.90}Pr_{0.10}O_2$, and $Ce_{0.80}Pr_{0.20}O_2$). X-ray diffraction confirmed the fluorite-like cubic crystal structure of the synthesized materials after heat treatment at 700 °C for 2 h. As-dried CeO_2 samples were found to have an average particle size of (6.0 ± 0.2) nm which increased to (17.0 ± 0.4) nm after heat treatment with an improvement in crystallinity. The particle size increased steadily with Pr content. The lattice parameter of Pr doped CeO_2 was found to increase or decrease with Pr content depending on the heat treatment process.

Keywords: Spray drying, CeO_2, Pr-doped CeO_2, XRD, TEM, EELS

1. Introduction

Rare-earth doped cerium oxides have recently become a potential alternative to the 'high temperature' zirconia based ceramics for solid oxide fuel cells (SOFCs) [1-3]. The attractive feature of these materials is their ability to show similar performance (higher ionic and electronic conductivities) at lower temperatures thereby improving overall energy efficiency, thermal stability and easy adaptation to cheaper counterparts in an SOFC [4-6]. Various methods have been reported to synthesize high surface area (HSA) nanoparticles of these materials including flame synthesis [7,8], sol-gel processing [9], homogenous precipitation [10] hydrothermal synthesis [11,12], mechanochemical synthesis [13], microwave assisted [14], and sonochemical synthesis [15]. The use of a 'spray route' which includes spray pyrolysis, spray drying and spray

freeze drying for nanosized particles has also been reported [16-21]. Nanopowders of mixed-oxide ceramics with homogenous chemical composition and high surface area have been successfully prepared by spray drying method [22-23]. Rare-earth doped ceria particles with micron sized particles have also been prepared recently using a commercially available spray drying system [24].

Spray drying is a relatively simple technique which is based on the atomization of an aqueous solution of the precursor and rapid evaporation of the solvent in a concurrent flow of hot air. Many techniques can be employed to produce a fine mist of droplets like ultrasonic nebulizer, electro-spray, spray nozzle, etc. Since the starting precursor is an aqueous mixture of the elemental salts, a homogeneous distribution of the mixed elements is expected with sufficiently rapid drying as compared to solid state mixing. Ideally one product particle (nanoparticle aggregate) should be generated from one droplet of the solution being atomized. This means that the final product particle size is dependent on the concentration and effective atomization of the starting precursor solution.

In this work, we report a simple laboratory scale spray dryer to synthesize Pr doped cerium oxide nanoparticles using an air brush for atomization. The spray dryer was custom built and provides an inexpensive alternative to commercially available spray dryers. The system can be used to synthesize a wide variety of pure as well as chemically homogeneous mixed oxide nanopowders compared to micron sized powders obtained using commercial spray dryers.

2. Experimental

Figures1 (a) and (b) respectively show a photograph and a schematic diagram of the spray drying system. Atomization of the liquid feed is achieved using a paint spray air brush with a 0.2 mm spray nozzle connected to the drying chamber as shown in Fig. 1(a). The liquid feed is introduced through the feed cup of the air-brush and is atomized by forcing compressed air through the nozzle resulting in a fine mist of droplets. The rate of atomization can be controlled by balancing the liquid feed rate to the airbrush and the flow of compressed air through its nozzle. The flow rate of the liquid feed was optimized to 0.7 cm^3/min making sure no excess liquid collects in the drying chamber and the solid product is formed almost instantaneously.

Drying was achieved using hot air generated by regulating air-heaters with built-in thermocouples and capable of reaching a maximum temperature of 760 °C. The air heaters are connected to the drying chamber via metal-to-glass connectors as seen at the right in Fig. 1(a). The temperature of the hot air can be controlled by varying the amount of current flowing through the heating element of the air-heater and/or air flow rate regulated by air-flow valve.

The drying chamber consists of an 8-inch diameter spherical shell made of glass. For our experiments, a maximum temperature of 350 °C inside the drying chamber was obtained using an air flow rate of 5.0 x 10^4 cm^3/min. This temperature is well below the softening temperature of glass vessel used (500 °C) and is sufficient for evaporation of water. The chamber also has multiple inlets so that the positions of the air-brush and hot air guns can be varied for optimum results. A suitable configuration of the air brush and the hot air guns can be obtained by analyzing the spray pattern and the properties of the as-dried product. The chamber is connected with a collector tube at the bottom marked as 'nanoparticle collection 1' in figure 1(b) to collect bigger agglomerates of the dried nanoparticles. Small sized agglomerates of the nanoparticles are carried away with the flowing air stream to the cyclone separator which is connected to the drying chamber via a swage-lock fitting. These smaller aggregates get separated from the air stream and are collected in another collector tube, marked as 'nanoparticle collection 2' in figure 1(b). The production rate of the solid phase is proportional to the flow rate of the liquid reactants and was found to be 0.015 g/min for pure ceria.

For our synthesis we prepared the starting precursor solutions by dissolving $Ce(NO_3)_3.6H_2O$ (cerium (III) nitrate hexahydrate; Alfa Aesar, 99.999%)*, and $Pr(NO_3)_3.6H_2O$ (praseodymium (III) nitrate hexahydrate; Alfa Aesar, 99.99%)* in de-ionized water. A 0.05 M solution was prepared by mixing these solutions in appropriate ratios to result in CeO_2, $Ce_{0.97}Pr_{0.03}O_2$, $Ce_{0.90}Pr_{0.10}O_2$, and $Ce_{0.80}Pr_{0.20}O_2$ nanoparticles after heat treatment. The mixed aqueous solutions were stirred for 30 min using a magnetic stirrer for homogenization. These solutions were then used as a liquid feed for the spray dryer. The spray dried powder was recovered by rinsing the glass chamber and the collector tubes with ethanol and drying in an oven overnight. Table 1 lists the types of heat treatments that were given to the samples. The spray drying process was designated as heat treatment 'A'. After the heat treatment A, the powder was subjected to heat

treatment ‘B’ in which it was heated to 700 °C for 2 h in air. For a comparison of the change in lattice parameter with the heat treatment process, the powder sample was also subjected to another heat treatment in which it was heated to 1000 °C for 10 h in air (heat treatment ‘C’).

The crystal structure of these samples was determined by x-ray diffraction using a Rigaku D/Max-IIB* diffractometer using Cu Kα radiation (λ = 1.5406 Å). Samples were loaded onto a zero background quartz plate and data collected over 2θ range of 20° to 100° and a step size of 0.02°. Lattice parameters were calculated using a least squares fitting procedure in JADE 9.0*. Particle size, nanoscale structure, crystallinity and chemical homogeneity were determined using a Tecnai F20* Transmission Electron Microscope (TEM) operated at 200 kV. Samples for the TEM investigation were prepared by dispersing the nanopowder in ethanol using an ultrasonicator to produce a dilute suspension. A standard holey carbon grid (carbon film supported on Cu grid) was immersed in the suspension and dried to produce the TEM sample. The particle size distribution was measured for a total of 300 particles using TEM image analysis. The chemical homogeneity of the synthesized nanoparticles was investigated by measuring the local concentration of Pr in the individual nanoparticles of Pr doped CeO_2 samples using electron energy loss spectroscopy (EELS). Energy loss spectroscopy was performed using a Gatan Imaging Filter (GIF)*.

3. Results and Discussion

The nanoparticles synthesized using the spray dryer were found to form agglomerates or clusters. These agglomerates are the result of multiple crystal nucleation sites in the super saturated salt solution formed as the droplet dries. As mentioned earlier, the size of this primary agglomerate depends on the concentration of the starting solution and the size of the atomized droplet. Additional aggregation between agglomerates may occur due to electrostatic interaction arising from charge on the primary liquid droplets leaving the spray nozzle.

Figures 2(a) and (b) show the TEM images of pure ceria nanopowders subjected to heat

Disclaimer: The full description of the procedures used in this paper requires the identification of certain commercial products and their suppliers. The inclusion of such information should in no way be construed as indicating that such products or suppliers are endorsed by NIST or are recommended by NIST or that they are necessarily the best materials, instruments, software or suppliers for the purposes described.

treatment A and heat treatment B respectively. The high resolution image in figure 2(a) shows amorphous regions indicating that the product obtained after spray drying was not fully crystallized. After subjecting the powder to heat treatment B, a considerable improvement in crystallinity was observed with no amorphous regions (figure 2(b)). The heat treatment step was necessary not only to improve crystallinity but also to fully decompose the nitrate precursors and to remove any residual moisture in the nanopowders after heat treatment A. The decomposition temperatures of cerium nitrate hexahydrate and praseodymium nitrate hexahydrate are 280 °C [25] and 465 °C [26] respectively. Also, since the maximum drying temperature in the spray dryer was kept at 350 °C to avoid degradation of its glass construction, heat treatment B was essential to complete precursor decomposition to oxide.

The average particle size of pure ceria nanopowder subjected to heat treatment A was found to be 6.0 nm ± 0.2 nm (with a standard deviation of 2 nm) which increased to 17.0 nm ± 0.4 nm (with a standard deviation of 6 nm) after heat treatment B. Figures 3(a) to 3(d) show the TEM images of CeO_2 and Pr-doped CeO_2 nanopowders after heat treatment B. Particle size analysis done using TEM images has been shown in figures 4(a) to 4(d). Mean particle size for $Ce_{0.97}Pr_{0.03}O_2$ and $Ce_{0.90}Pr_{0.10}O_2$ samples was found to be 22.0 nm ± 0.4 nm (with a standard deviation of 7 nm) and 22.0 nm ± 0.4 nm (with a standard deviation of 7 nm) respectively. However, the mean particle size for $Ce_{0.80}Pr_{0.20}O_2$ sample was found to be slightly larger, 33.0 nm ± 0.5 nm (with a standard deviation of 9 nm).

The Pr concentration in individual nanoparticles was measured using an EELS procedure which will be reported in detail elsewhere [27]. The coefficient of variation (CV), i.e. the ratio of standard deviation to the mean was used as a measure of ‘chemical heterogeneity’. Figures 5 (a) and 5(b) show the local concentration of Pr in individual nanoparticles of $Ce_{0.97}Pr_{0.03}O_2$ after heat treatment A and heat treatment B respectively. The mean Pr concentration after heat treatment A was found to be 0.031 with a standard deviation of 0.012 and coefficient of variation equal to 39%. After subjecting the nanoparticles to heat treatment B, the mean Pr concentration was found to be 0.032 with a standard deviation of 0.007. The coefficient of variation in this case was found to be 20%. This shows that the sample became more homogenous after the heat treatment B. Figures 5(c) and 5(d) show the local concentration of Pr in the individual nanoparticles of

$Ce_{0.90}Pr_{0.10}O_2$ and $Ce_{0.80}Pr_{0.20}O_2$ after heat treatment B. The mean Pr concentration in the former was found to be 0.093 with a standard deviation of 0.011 and a coefficient of variation equal to 11%. In the latter case, the mean Pr concentration was found to be 0.200 with a standard deviation of 0.058 and a coefficient of variation equal to 29%. The $Ce_{0.90}Pr_{0.10}O_2$ sample having the lowest coefficient of variation was hence the least heterogeneous and the $Ce_{0.80}Pr_{0.20}O_2$ sample with the highest coefficient of variation the most.

X-ray diffraction patterns obtained for CeO_2 and Pr-doped CeO_2 nanoparticles after heat-treatment B are as shown in Fig. 6. A fluorite-like cubic crystal structure was obtained for both pure CeO_2 and Pr doped CeO_2 compositions, in accordance with the X-ray powder diffraction file (JCPDS 34-394). The inset in figure 5 shows a peak shift to lower 2-theta angles observed for (331) and (420) Bragg reflections in the Pr-doped CeO_2 samples in comparison with pure CeO_2. The peak shift indicates the incorporation of the Pr dopant into the host CeO_2 lattice along with a change in lattice parameter. The observed value of lattice parameter of spray dried and calcined pure CeO_2 was found to be 0.5409 nm. This value is slightly smaller than the value reported in literature of 0.541134 nm [JCPDS 34-394]. Fig. 7(a) shows the change in lattice parameter of Pr doped CeO_2 with increasing Pr concentration for samples subjected to heat treatment B. It was found that the lattice parameter increased with Pr concentration in CeO_2 where it seemed to follow a Vegard's type behavior up to Pr concentration of 0.10. The $Ce_{0.80}Pr_{0.20}O_2$ composition however seemed to deviate from this linearity, possibly due to being relatively more heterogeneous. The increase in lattice parameter with Pr content is an indication that most of the Pr ions were present in 3+ oxidation state (ionic radii of eight-fold coordinated Pr^{3+} is 0.1126 nm as compared to 0.097 nm for Ce^{4+} [28]. The observed trend in lattice parameter change with composition is in agreement with that reported by Shuk et al. [29], Sadykov et al. [34], and Borchert et al. [35], where the samples subjected to low temperature heat treatment were found to obey Vegard's law owing to the presence of the larger Pr^{3+} ions. However, an opposite trend was observed by Nauer et al. [30] and Takasu et al. [31], where lattice parameter was found to decrease with increasing amount of doping. The discrepancy can be explained based on the fact that the valence state of Pr can vary according to the type of heat treatment

given to the sample [32-33]. The findings of Takasu et al. were based on the samples sintered in air at 1400 °C and the decrease in lattice parameter was associated with the presence of Pr^{4+} ions.

The value of lattice parameter of pure CeO_2 subjected to heat treatment B was found to be 0.04% smaller than the accepted value in literature. However, the lattice parameter of CeO_2 sample subjected to heat treatment C was found to be 0.5411 nm which is in close agreement to the value reported in the literature. Figure 7(b) shows the change in lattice parameter of CeO_2 with Pr after heat treatment C. A decrease in the lattice parameter with increasing Pr content was observed and agrees qualitatively with the findings of Nauer et al. and Takasu et al. This decrease is attributed to the oxidation of Pr^{3+} ions to Pr^{4+} at 1000 °C in air (ionic radii of Pr^{4+} ion being 0.096 nm which is slightly smaller than Ce^{4+} ions (0.097 nm)). The nonlinearity can be explained on the basis of residual amounts of Pr^{3+} ions present at room temperature after sintering which affects the lattice parameter of CeO_2 to different levels with Pr content.

4. Conclusion

Mixed oxide nanoparticles of Pr doped ceria were successfully synthesized using a simple custom built spray dryer. A fluorite type cubic crystal structure was obtained after heat treatment as evidenced by X-ray diffraction. TEM analysis showed that the crystallinity and nanoscale compositional heterogeneity improved considerably after heat treatment. The EELS analysis showed that the compositional heterogeneity was in the range of 10% to 30% based on the coefficient of variation. The lattice parameter of the Pr doped CeO_2 subjected to low temperature heat treatment was found to increase with Pr content owing to the presence of Pr^{3+} ions. However, after high temperature heat treatment, the lattice parameter was found to decrease non-linearly with Pr content and was attributed to the oxidation of Pr^{3+} to Pr^{4+} ions which are smaller in size. This spray dryer can be used to synthesize a wide variety of pure as well as doped nanomaterials.

Acknowledgements

We gratefully acknowledge the support from the US Department of Energy (DE-FG02-07ER46442) and John M. Cowley Center for High Resolution Microscopy at Arizona State University.

References

[1] A. Atkinson, S. Barnett, R.J. Gorte, J.T.S. Irvine, A.J. Mcevoy, M. Mogensen, S. C. Singhal and J, Vohs, Nature Materials 3 (2004) 17.

[2] A. Trovarelli, Catalysis by Ceria and Related Materials, Imperial College Press, London, 2002.

[3] B.C.H. Steele, A. Heinzel, Nature 414 (2001) 345.

[4] David A. Andersson, Sergei I. Simak, Natalis V. Skorodumova, Igor A. Abrikosov, and Borje Johansson, PNAS 103 (2006) 10.

[5] Y. Takasu, T. Sugino, Y. Matsuda, J. Appl. Electrochem., 14 (1984) 79.

[6] M. Nauer, C. Ftikos, and B.C.H. Steele, J. Eur. Ceram. Soc., 14 (1994) 493.

[7] L. Mädler, W. J. Stark and S.E. Pratsinis, J. Mater. Res. 17 (2002) 1356.

[8] H. K. Kammler, L. Mädler, and S. E. Pratsinis, Chem. Eng. Technol. 24 (2001) 6 pp. 583-596.

[9] C.K. Narula, L.P. Haack, W. Chun, H.-W. Jen, and G.W. Graham, J. Phys. Chem. B. 103 (1999) 3634.

[10] T. C. Rojas, and M. Ocana, Scripta Mater. 46 (2002) 655.

[11] A. I. Y. Tok, S.E. Du, F.Y.C. Boey, and W. K. Chong, Mat. Sci. Eng. A 466 (2007) 223.

[12] T. Masui, H. Hirai, N. Imanaka, G. Adachi, T. Sakata, and H. Mori, J. Mater. Sci. Lett. 21 (2002) 489.

[13] T. Tsuzuki, and P.G. McCormick, J. Mater. Sci. 39 (2004) 5143.

[14] H. Yang, C. Huang, A. Tang, X. Zhang, and W. Yang, Mater. Res. Bull. 40(2005) 1690.

[15] L.Yin, Y. Wang, G. Pang, Y. Koltypin, and A. Gedanken, J. Colloid Interface Sci. 246 (2002) 78.

[16] K. Okuyama and I.W. Lengorro, Chem. Eng. Sci. 58 (2003) 537.

[17] L.C. Chow, L. Sun, and B. Hockey, J. Res. Natl. Inst. Stand. Technol. 109 (2004) 543.

[18] F. Iskandar, L. Grandon, and K. Okuyama, J. Colloid Interface Sci. 265 (2003) 296.

[19] Y.Li, C. Wan, Y. Wu, C. Jiang, and Y. Zhu, J. Power Sources, 85 (2000) 294.

[20] T.S. Lyubenova, F. Matteucci, A. Costa, M. Dondi, and J. Carda, Powder Technol. 193 (2009) 1.

[21] R. Wang, P.A. Crozier, R. Sharma, and J. B Adams, J. Phys. Chem B 110(2006) 18278.

[22] H.M. Wu, J.P. Tu, Y.Z. Yang, and D.Q. Shi, J. Mater. Sci. 41 (2006) 4247.

[23] I.V. Driescche, B. Schoofs, E. Bruneel, and S. Hoste, J. Eur. Ceram. Soc. 24 (2004) 1823.

[24] P. Blennow, W. Chen, M. Lundburg, and M. Menon, Ceram. Int. 35 (2009) 2959.

[25] E.A. Strydom and C.P.J. van Vuuren, J. Therm. Anal., 32 (1987) 157.

[26] G.A.M. Hussein, B.A.A. Balboul, M.A.A-Warith, A.G.M. Othman, Thermochim. Acta, 369 (2001) 59.

[27] V. Sharma, K. R. Sharma, J. B. Adams and P.A. Crozier, to be published.

[28] R.D. Shannon, Acta Cryst. A32 (1976) 751.

[29] P. Shuk, M. Greenblatt, Solid State Ionics 116 (1999) 217.

[30] M. Nauer, C. Ftikos, B.C.H. Steele, J. Eur. Ceram. Soc. 14 (1994) 493.

[31] Y. Takasu, T. Sugino, Y. Matsuda, J. Appl. Electrochem. 14 (1984) 79.

[32] K.G. Gartsman, N.F. Kartenko, B.T. Melekh, S.V. Nikitin, I.A. Smirnov, Y.N. Filin, N.V. Sharenkova, A.T. Shuvaev, B.Y. Khel'mer, F.M. Ovsyannikov, Sov. Phys. Solid State 32 (1990) 1089.

[33] A.E. Sovestnov, V.A. Shaburov, B.T. Melekh, I.A. Smirnov, Y.P Smirnov, A.V. Tyunis, A.I. Egorov, Phys. Solid State 36 (1994) 620.

[34] V.A. Sadykov, Yu.V. Frolova, G.M. Alikina, A.I. Lukashevich, V.S. Muzykantov, V.A. Rogov, E.M. Moroz, D.A. Zyuzin, V.P. Ivanov, S.N. Trukhan, V.I. Zaikovski, H. Borchert, E.A. Paukshtis, V.I. Bukhtiyarov, V.V. Kaichev, I.P.Prosvirin, S. Neophytides, E. Kemnitz, K. Scheurell, *React. Kinet. Catal. Lett*., 86 (2005) 1, 21

[35] H. Borchert, Yu.V. Frolova, V.V. Kaichev, I.P. Prosvirin, G.M. Alikina, A.I.Lukashevich, V.I. Zaikovski, E.M. Moroz, S.N. Trukhan, V.P. Ivanov, E.A. Paukshtis, V.I. Bukhtiyarov, and V.A. Sadykov, J. Phys. Chem. B 2005, 109, 5728.

Figure Captions

Fig1. (a) Photograph of the spray dryer for nanoparticle synthesis, and (b) schematic representation of the spray drying system.

Fig2. High resolution TEM micrographs of CeO_2 obtained after (a) heat treatment A, and (b) heat treatment B.

Fig3. TEM micrographs of (a) CeO_2, (b) $Ce_{0.97}Pr_{0.03}O_2$, (c) $Ce_{0.90}Pr_{0.10}O_2$ and (d) $Ce_{0.80}Pr_{0.20}O_2$ nanoparticles after heat treatment B.

Fig4. Particle size distributions for (a) CeO_2, (b) $Ce_{0.97}Pr_{0.03}O_2$, (c) $Ce_{0.90}Pr_{0.10}O_2$, and (d) $Ce_{0.80}Pr_{0.20}O_2$ nanoparticles after heat treatment B.

Fig5. Compositions of individual nanoparticles of (a) $Ce_{0.97}Pr_{0.03}O_2$ after heat treatment A, (b) same composition after heat treatment B, (c) and (d) $Ce_{0.90}Pr_{0.10}O_2$ and $Ce_{0.80}Pr_{0.20}O_2$ respectively, after heat treatment B.

Fig6. X-ray diffraction patterns for Pr-doped CeO_2 after heat treatment B. Inset: Observed peak shift for (331) and (420) reflection.

Fig7. Change in lattice parameter of CeO_2 with Pr concentration after (a) heat treatment B, and (b) after heat treatment C.

FIG 1A

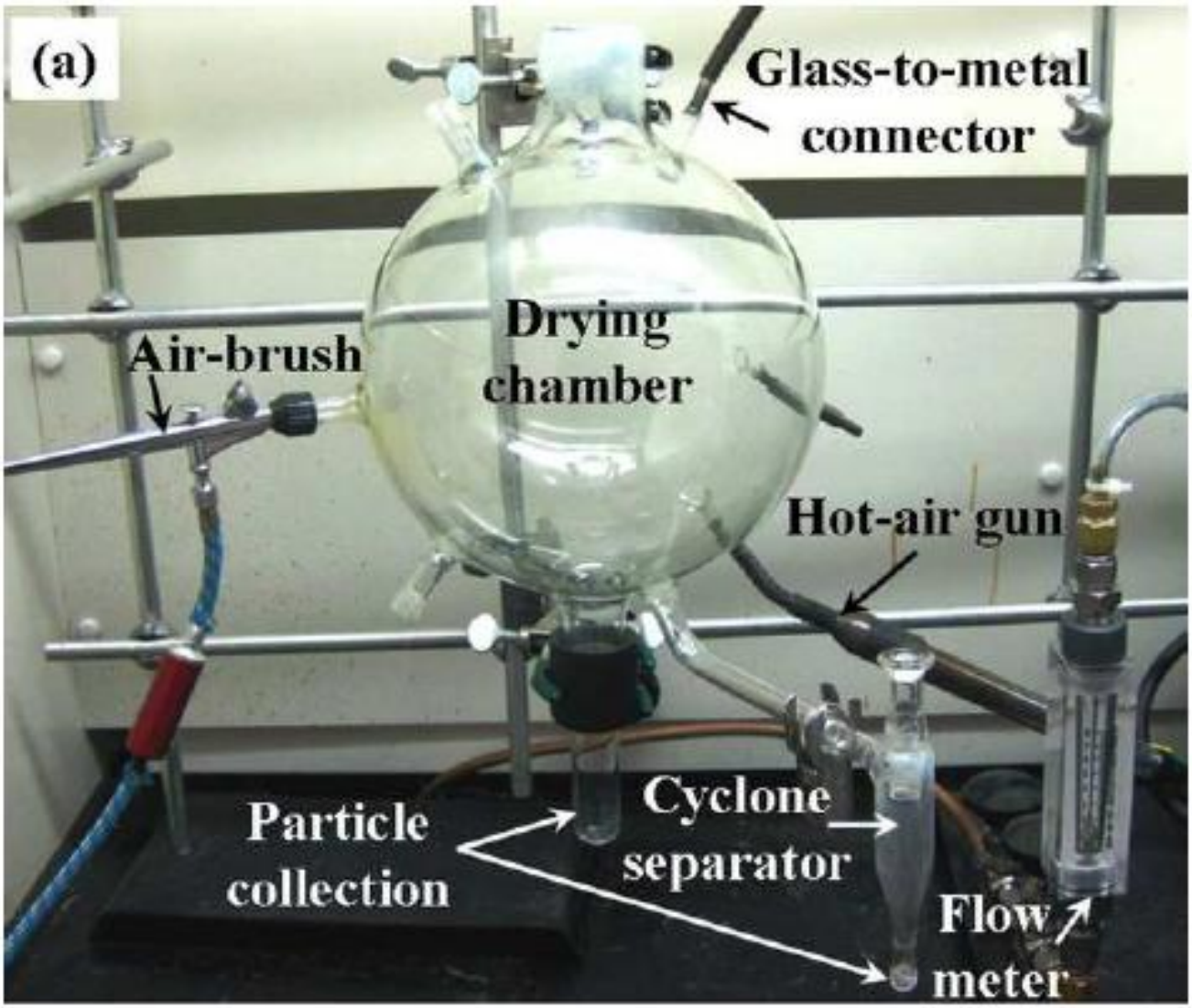
(a)
Glass-to-metal connector
Drying chamber
Air-brush
Hot-air gun
Particle collection
Cyclone separator
Flow meter

FIG 1B

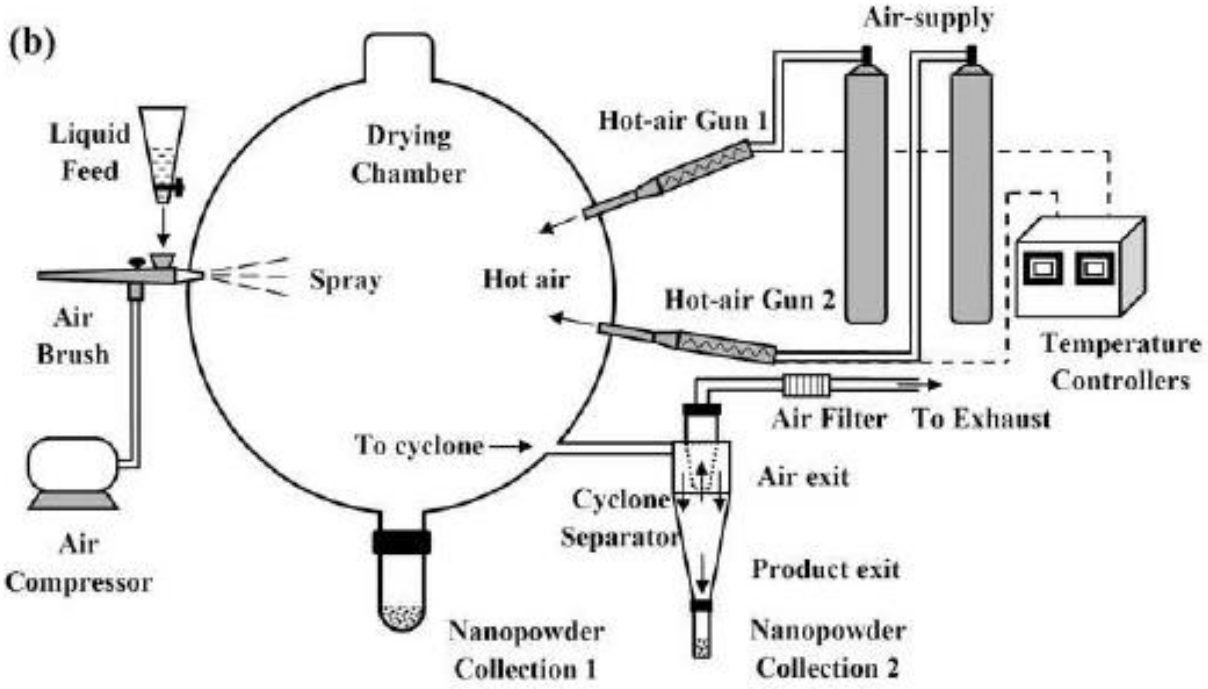
(b)
Air-supply
Liquid Feed
Drying Chamber
Hot-air Gun 1
Spray
Hot air
Hot-air Gun 2
Air Brush
Temperature Controllers
Air Filter
To Exhaust
To cyclone
Air exit
Cyclone Separator
Air Compressor
Product exit
Nanopowder Collection 1
Nanopowder Collection 2

FIG 2A

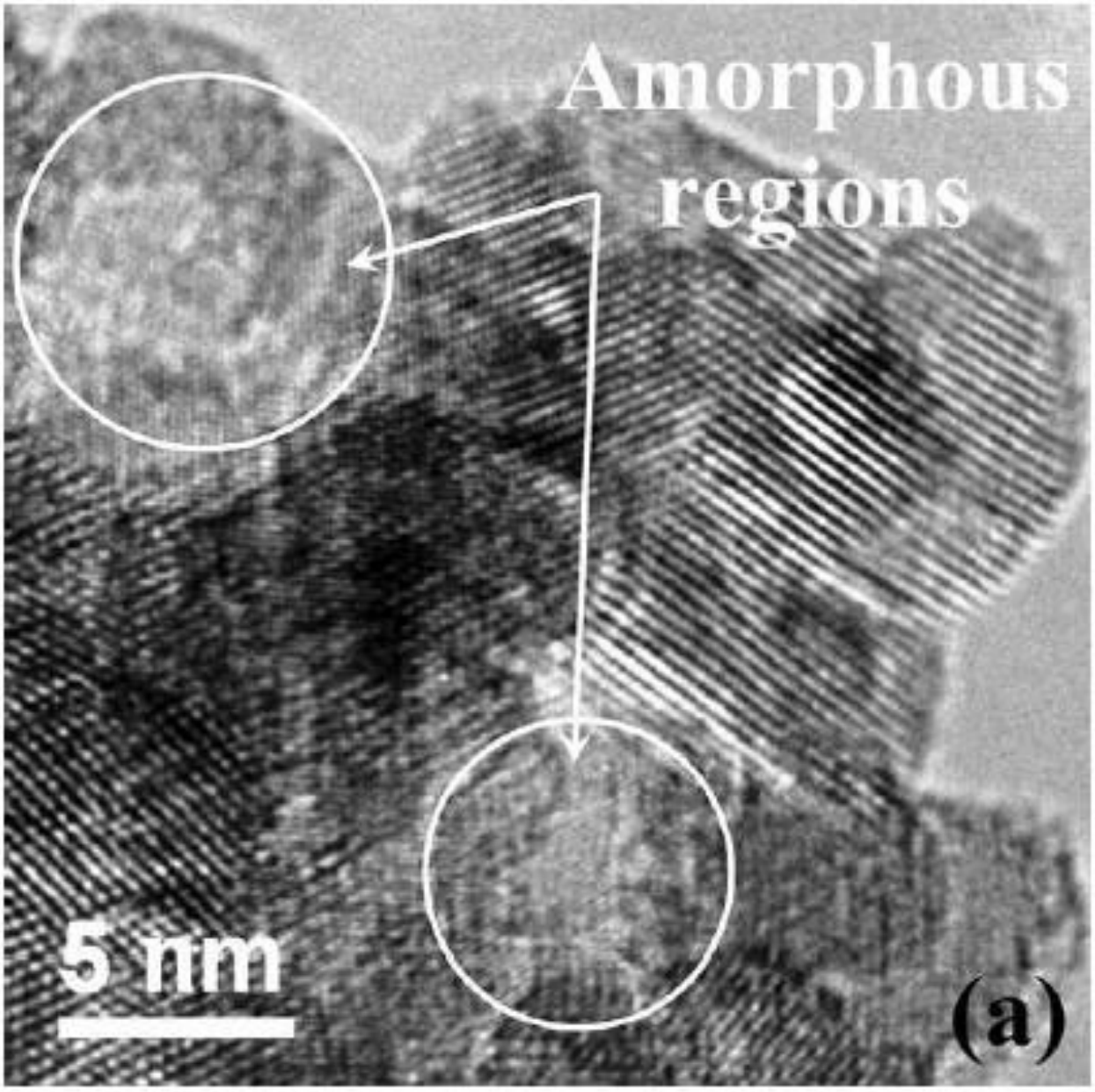

FIG 2B

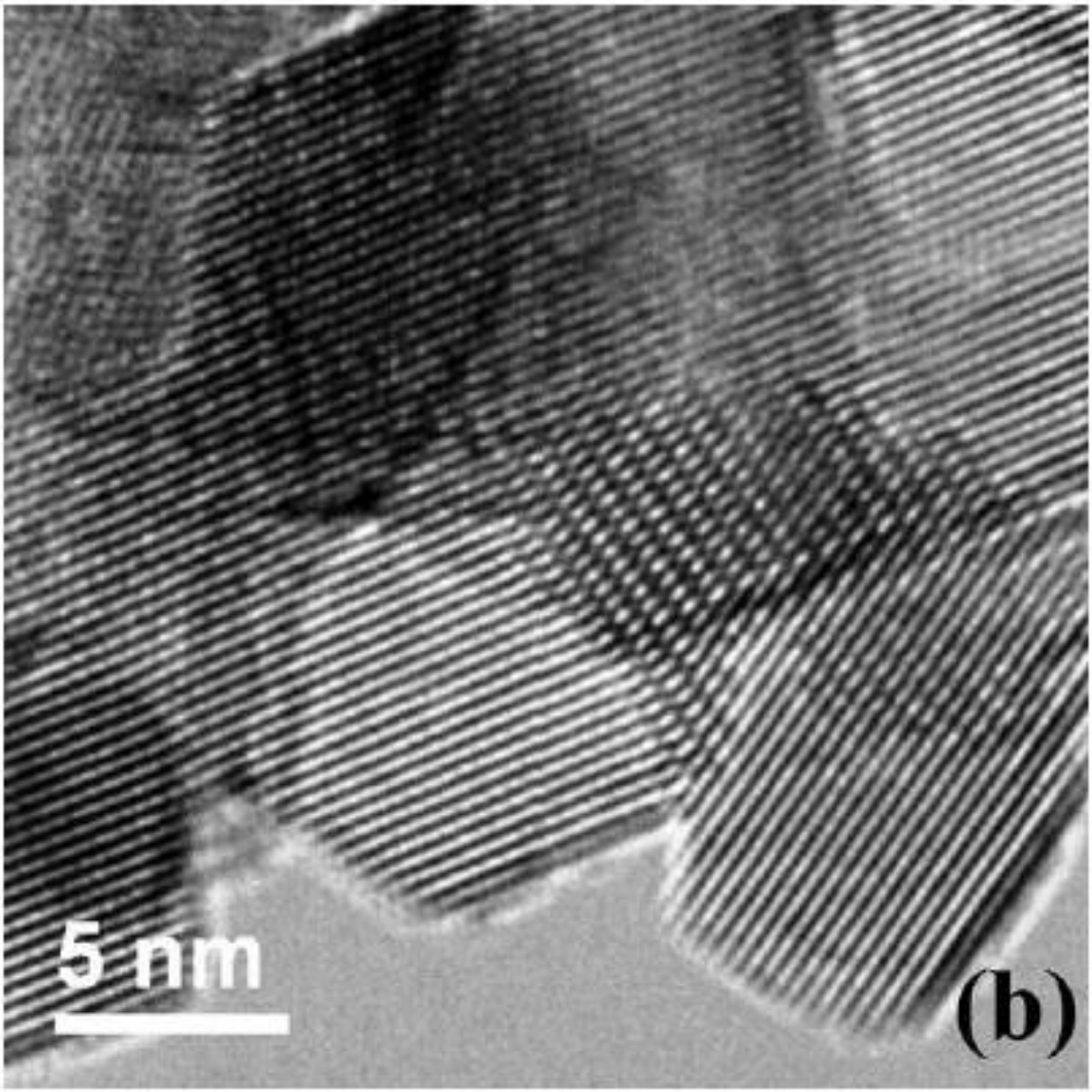

FIG 3A

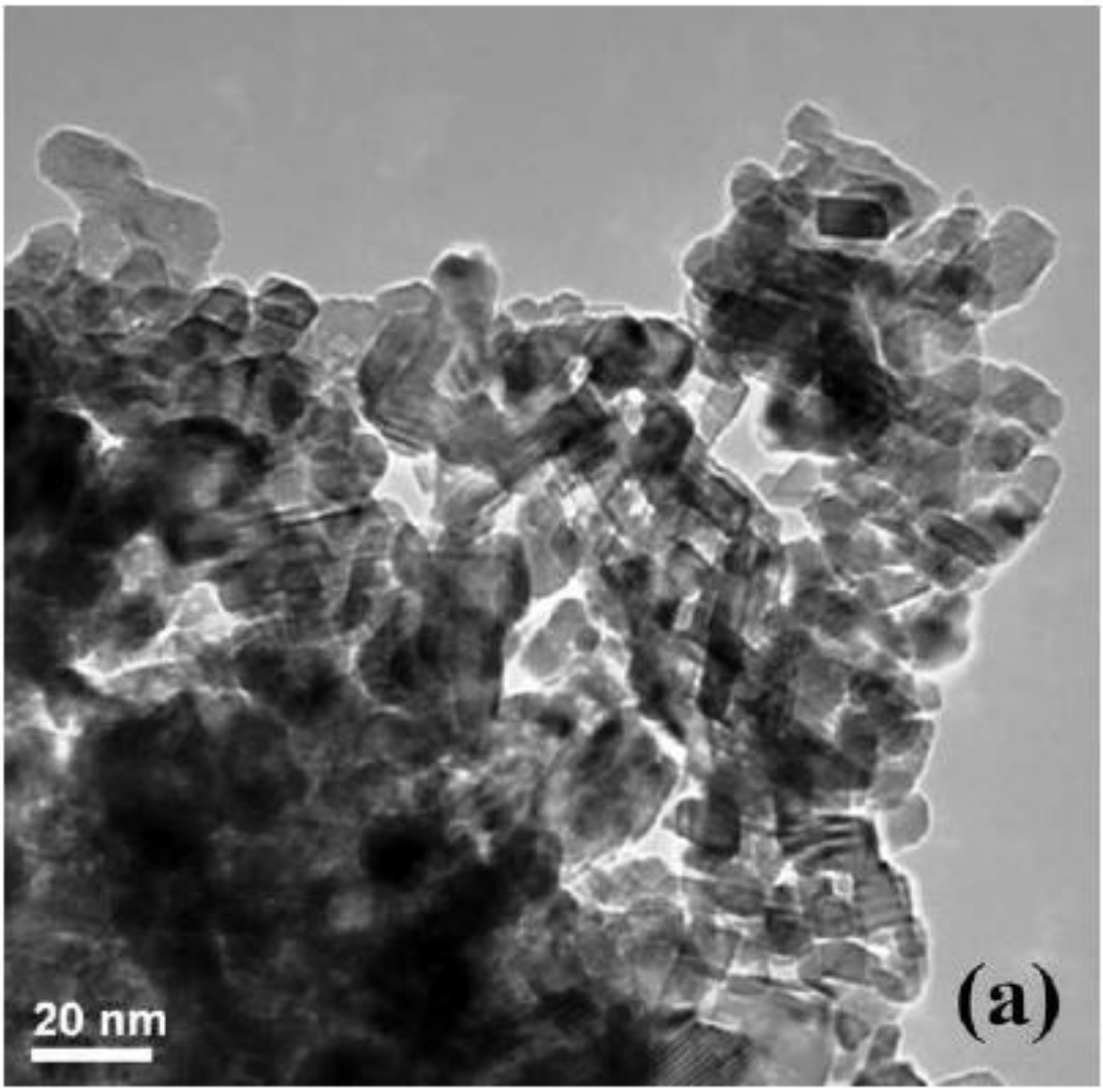

FIG 3B

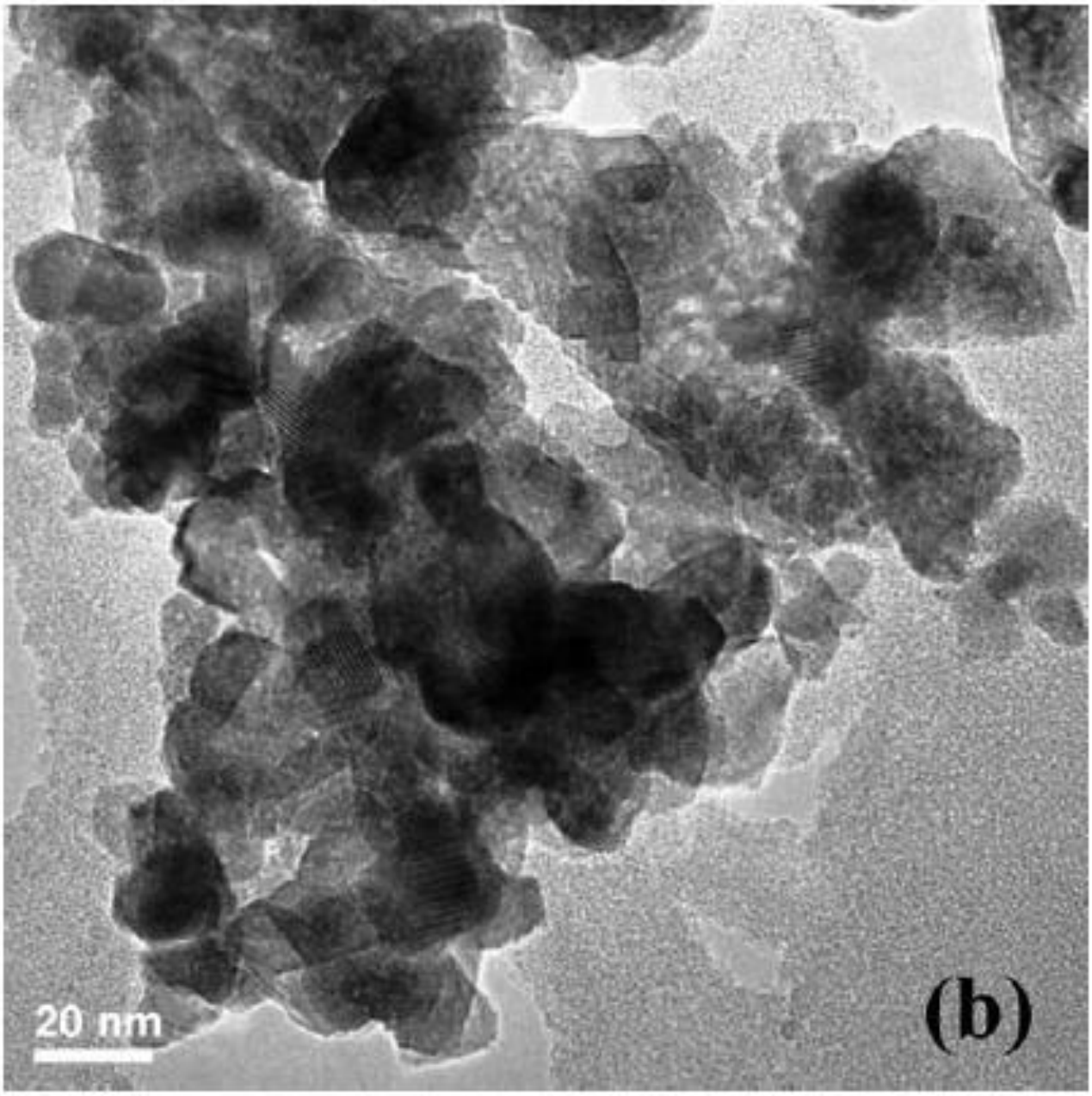

FIG 3C

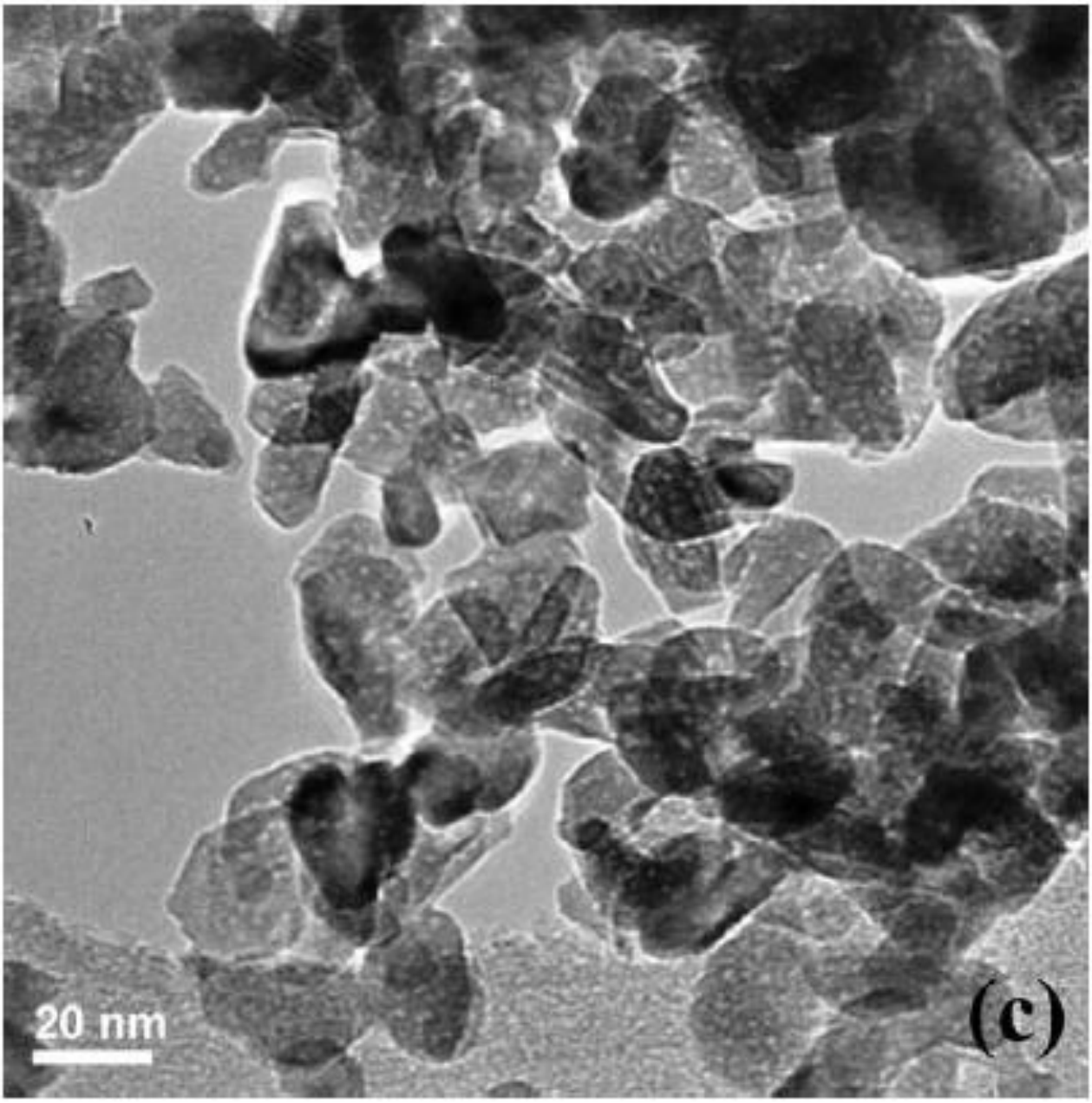

FIG 3D

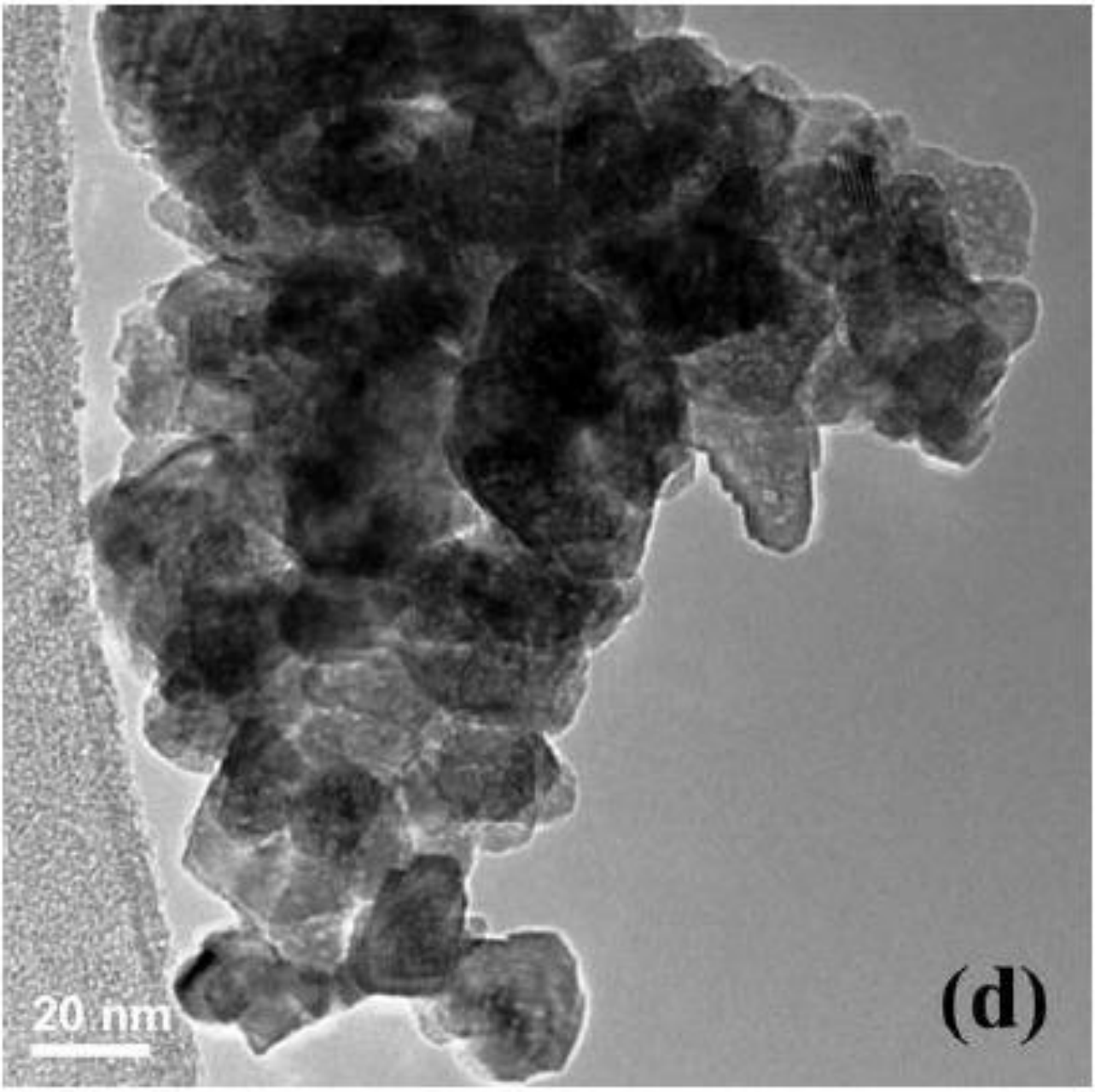

FIG 4A

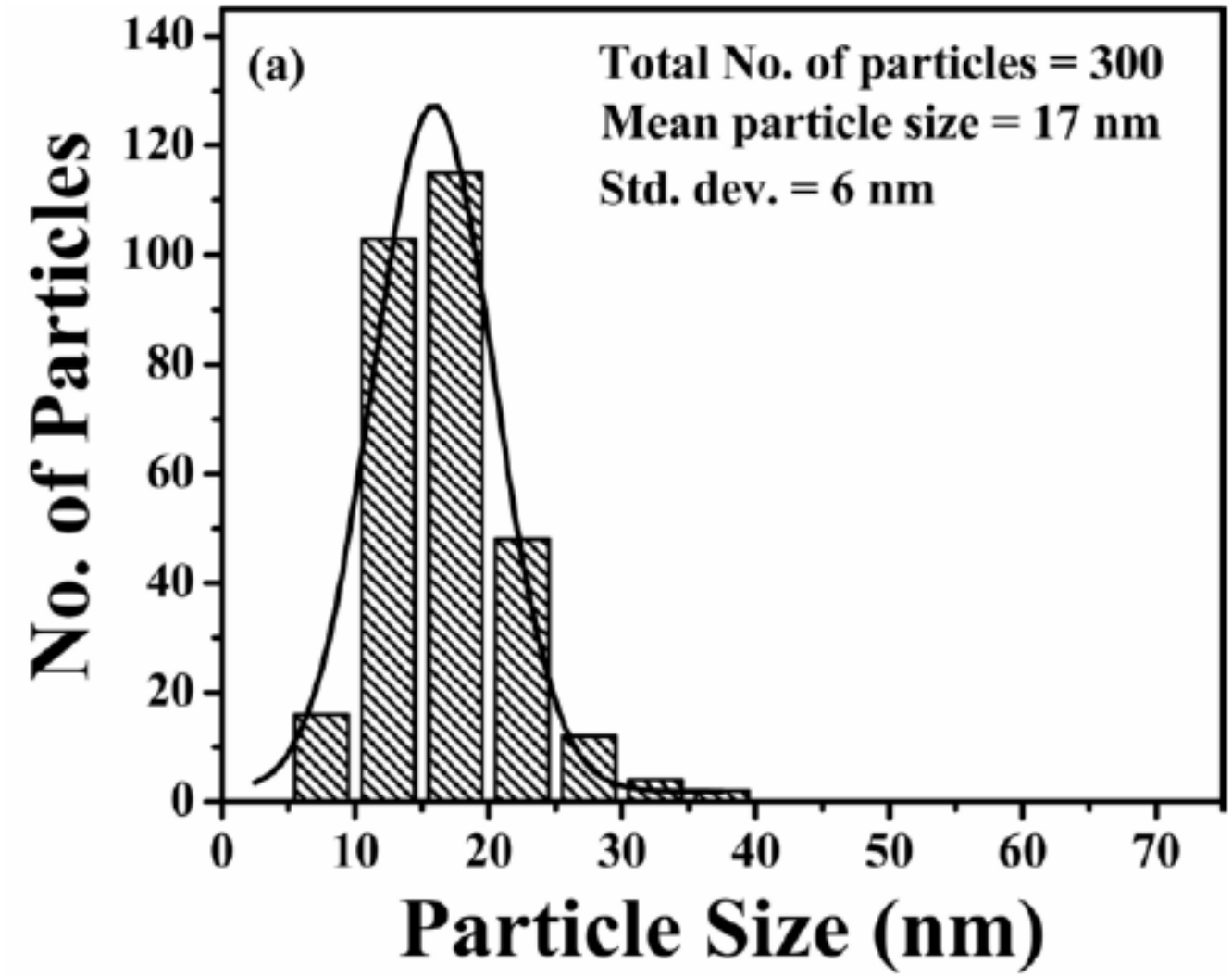
(a)
Total No. of particles = 300
Mean particle size = 17 nm
Std. dev. = 6 nm
No. of Particles
Particle Size (nm)
0
20
40
60
80
100
120
140
0
10
20
30
40
50
60
70

FIG 4B

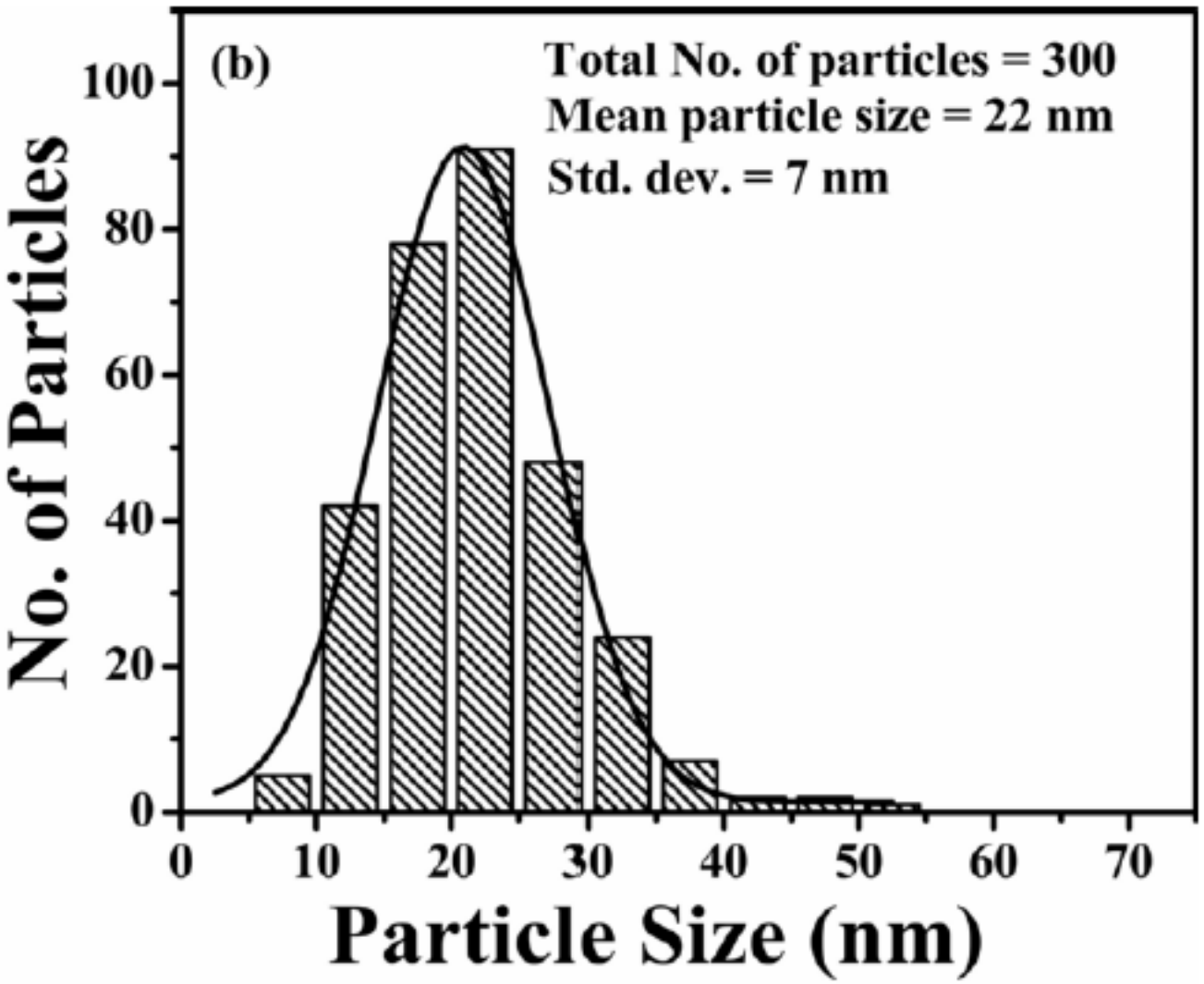
(b)
Total No. of particles = 300
Mean particle size = 22 nm
Std. dev. = 7 nm
No. of Particles
0
20
40
60
80
100
0
10
20
30
40
50
60
70
Particle Size (nm)

FIG 4C

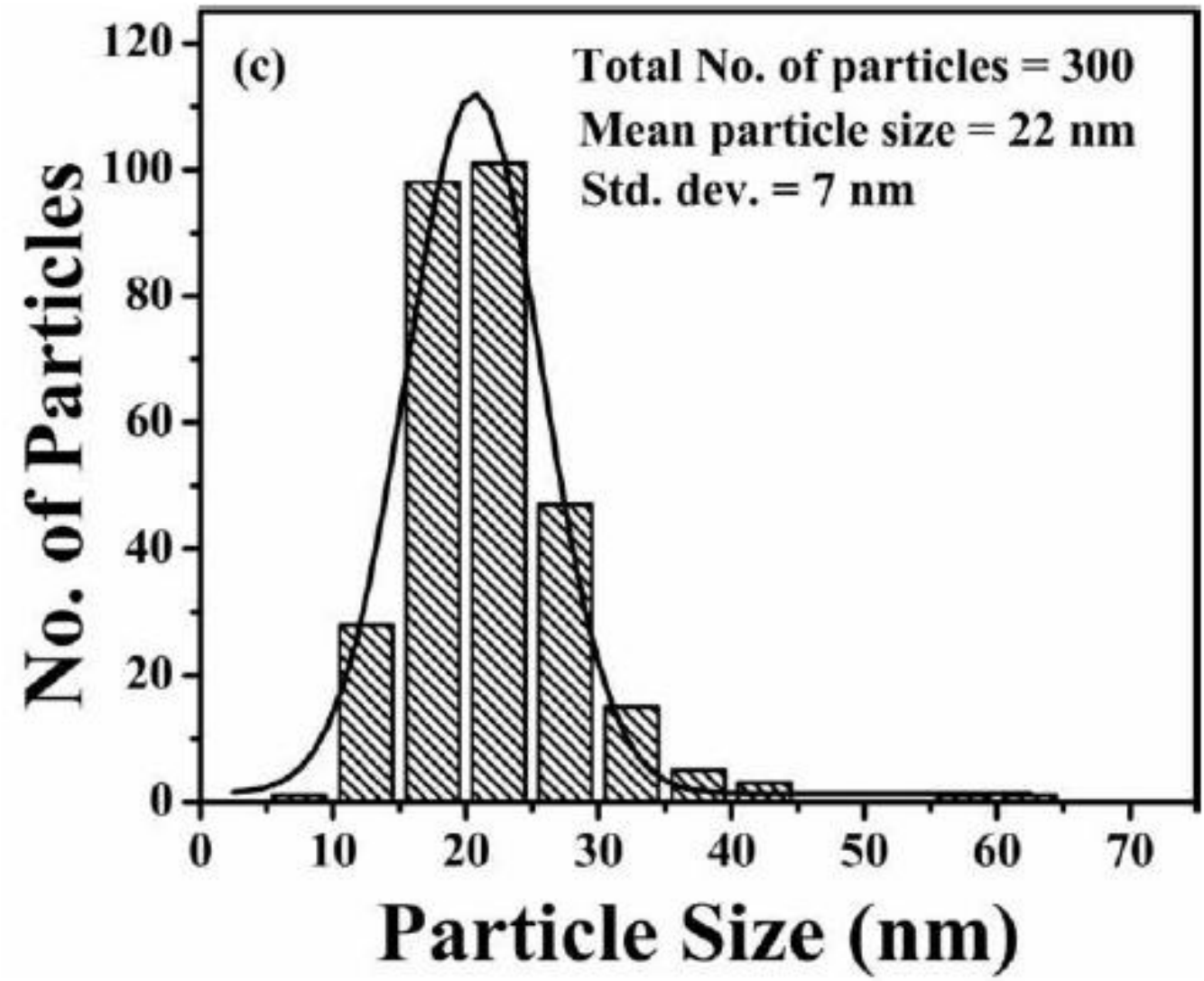
(c)
Total No. of particles = 300
Mean particle size = 22 nm
Std. dev. = 7 nm
No. of Particles
Particle Size (nm)
0
20
40
60
80
100
120
0
10
20
30
40
50
60
70

FIG 4D

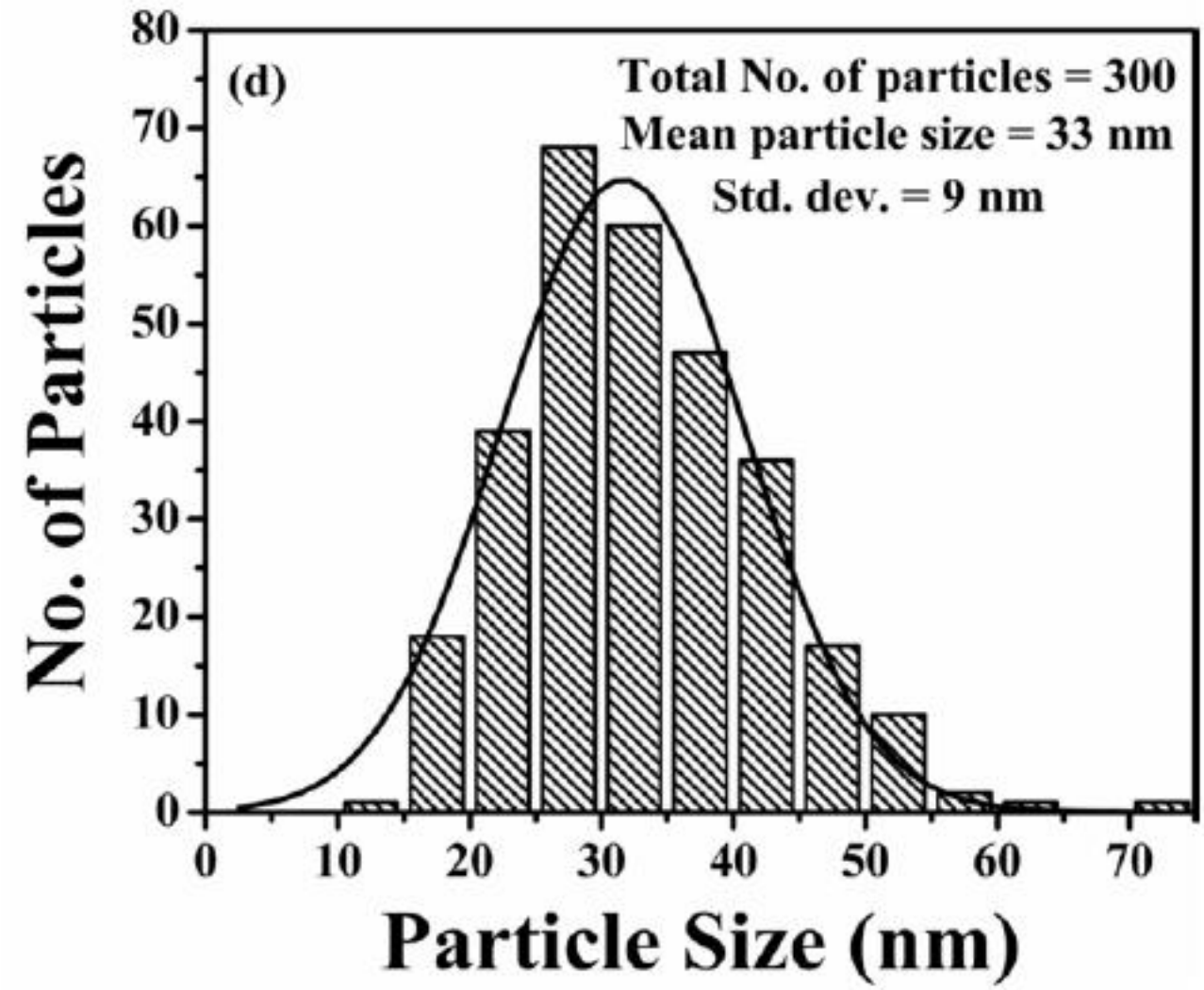
(d)
Total No. of particles = 300
Mean particle size = 33 nm
Std. dev. = 9 nm
No. of Particles
Particle Size (nm)
0
10
20
30
40
50
60
70
80

FIG 5A

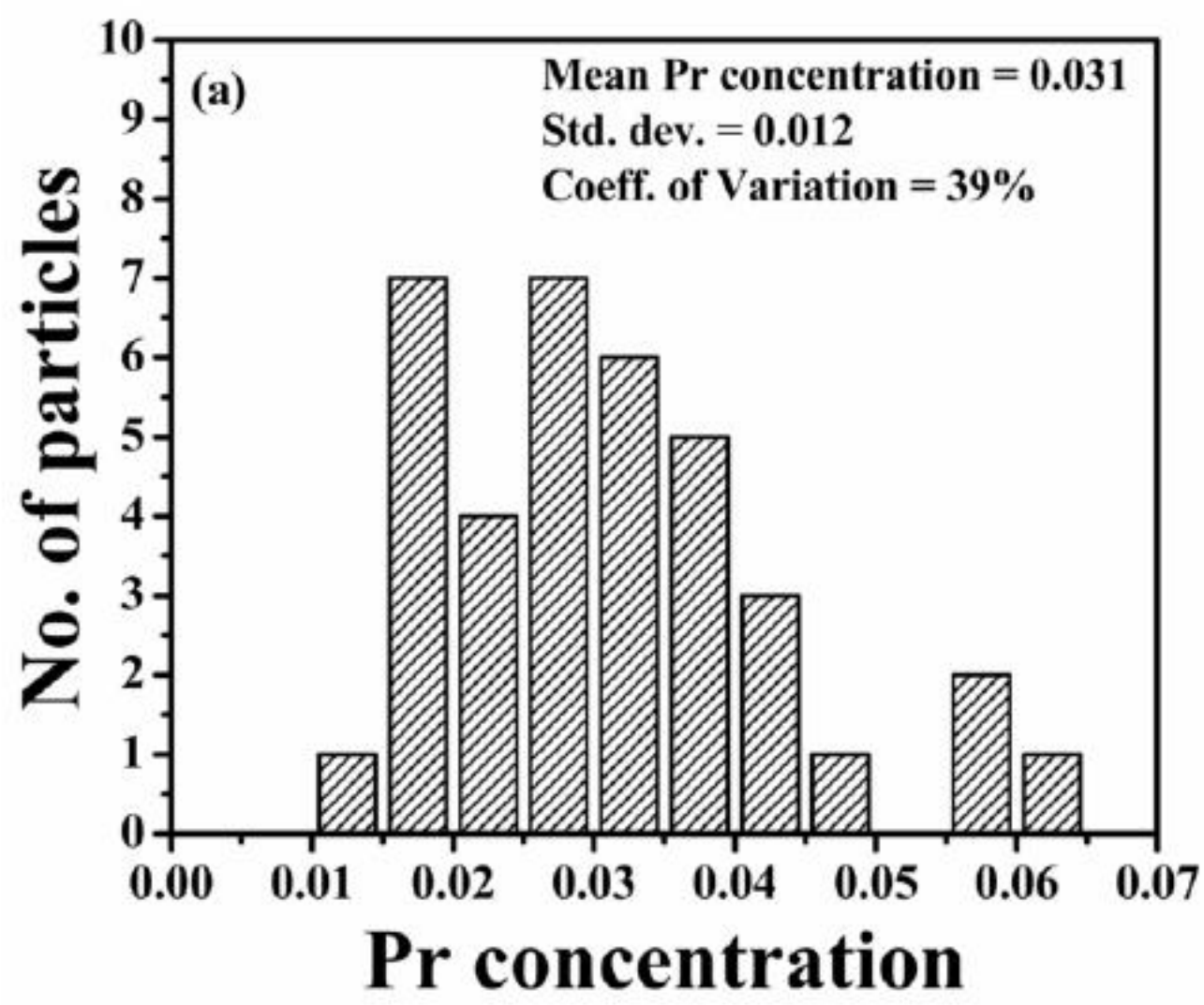
(a)
Mean Pr concentration = 0.031
Std. dev. = 0.012
Coeff. of Variation = 39%
No. of particles
Pr concentration
0
1
2
3
4
5
6
7
8
9
10
0.00
0.01
0.02
0.03
0.04
0.05
0.06
0.07

FIG 5B

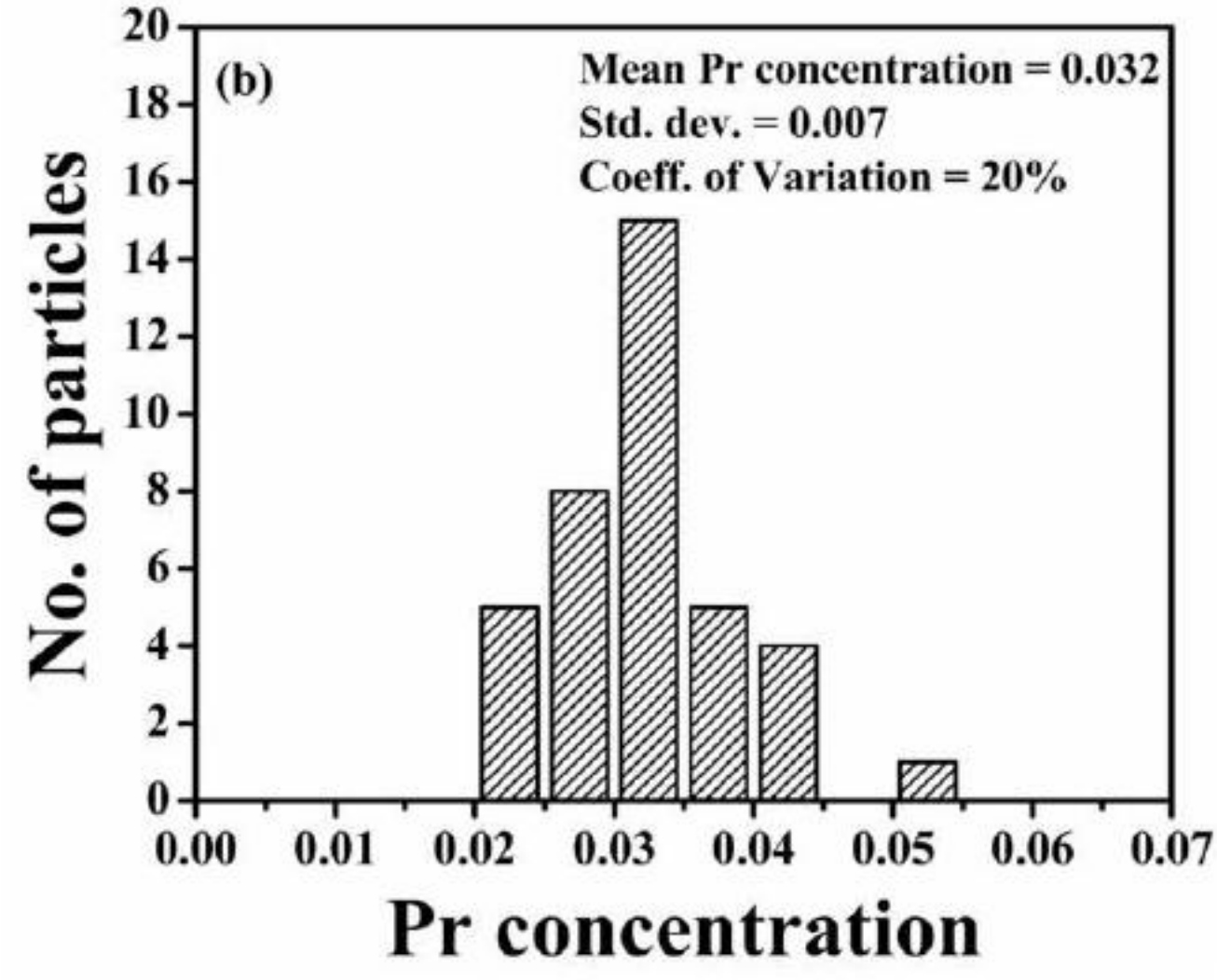
(b)
Mean Pr concentration = 0.032
Std. dev. = 0.007
Coeff. of Variation = 20%
No. of particles
Pr concentration
0
2
4
6
8
10
12
14
16
18
20
0.00
0.01
0.02
0.03
0.04
0.05
0.06
0.07

FIG 5 C

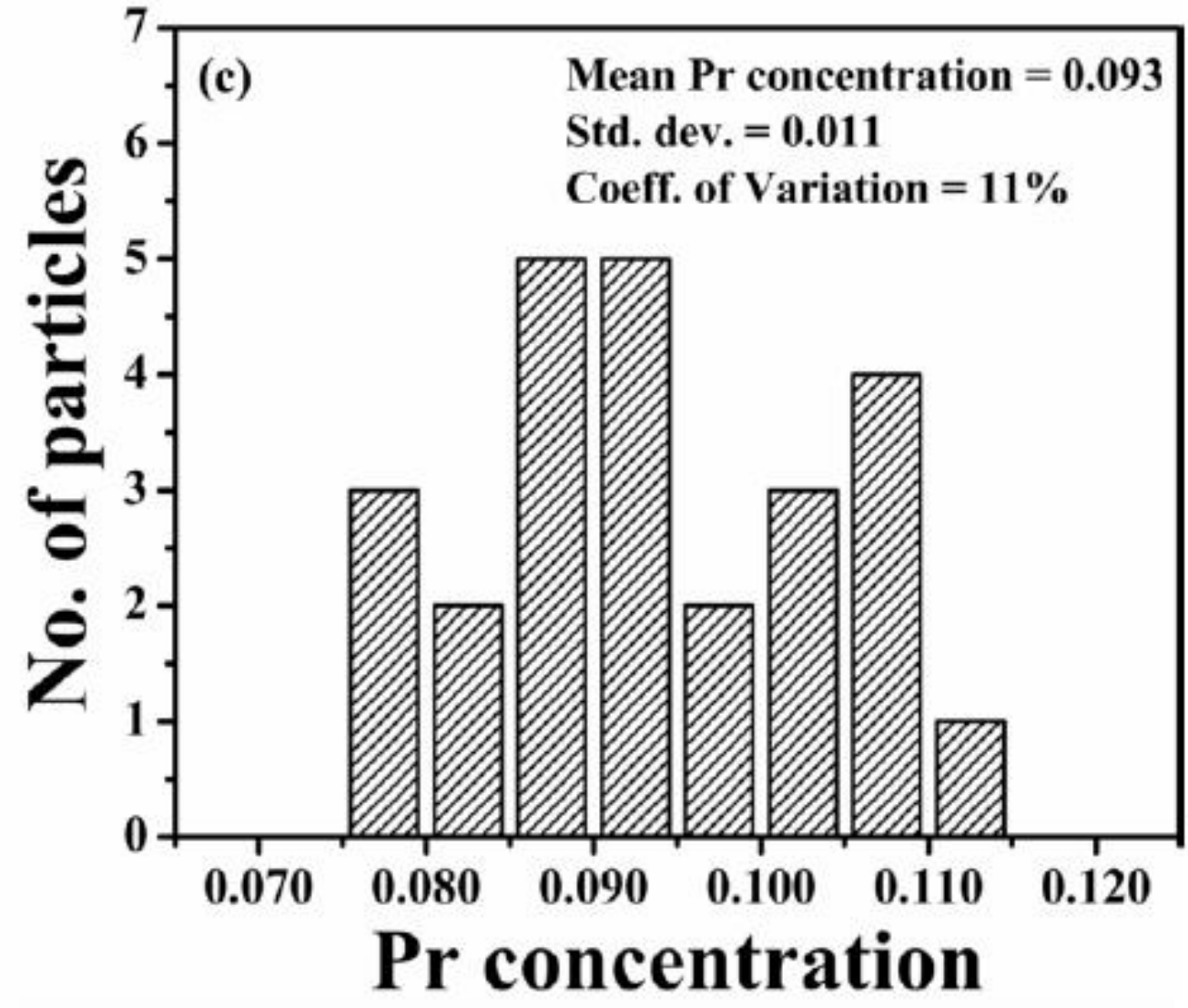
(c)
Mean Pr concentration = 0.093
Std. dev. = 0.011
Coeff. of Variation = 11%
No. of particles
0
1
2
3
4
5
6
7
0.070
0.080
0.090
0.100
0.110
0.120
Pr concentration

FIG 5D

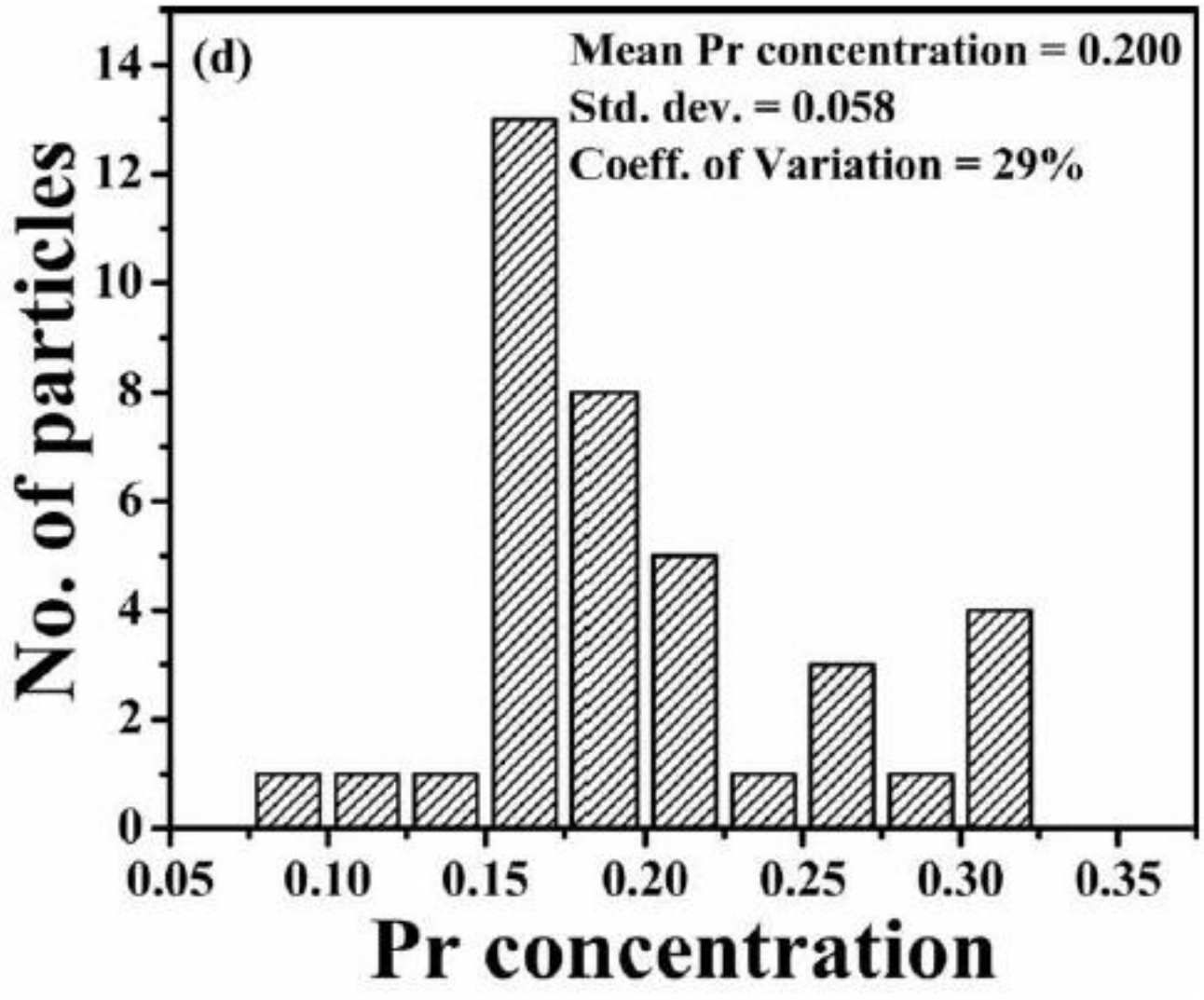
(d)
Mean Pr concentration = 0.200
Std. dev. = 0.058
Coeff. of Variation = 29%
No. of particles
0
2
4
6
8
10
12
14
0.05
0.10
0.15
0.20
0.25
0.30
0.35
Pr concentration

FIG 6

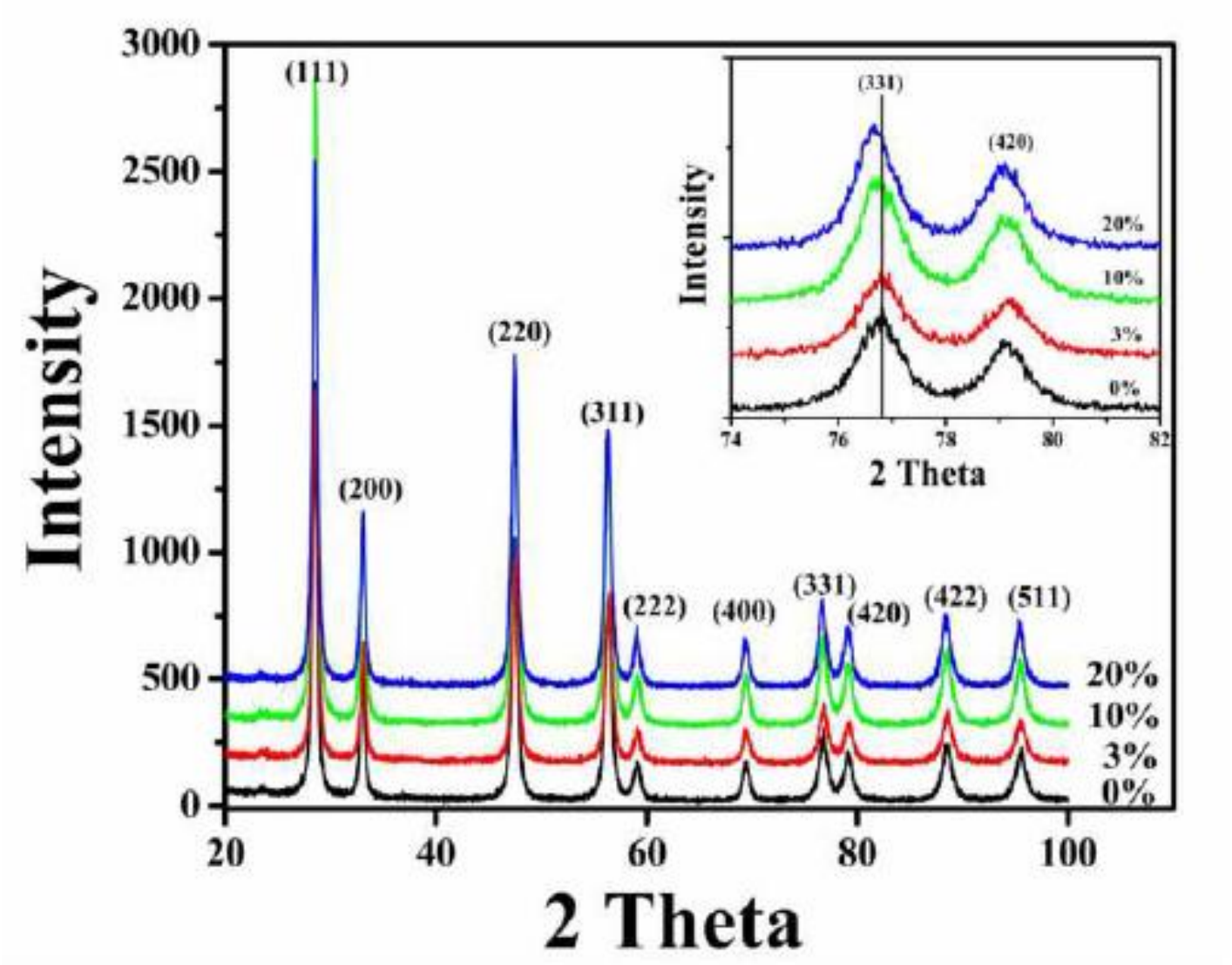
Intensity
2 Theta
(111)
(200)
(220)
(311)
(222)
(400)
(331)
(420)
(422)
(511)
20%
10%
3%
0%
Intensity
2 Theta
(331)
(420)
20%
10%
3%
0%

FIG 7 A

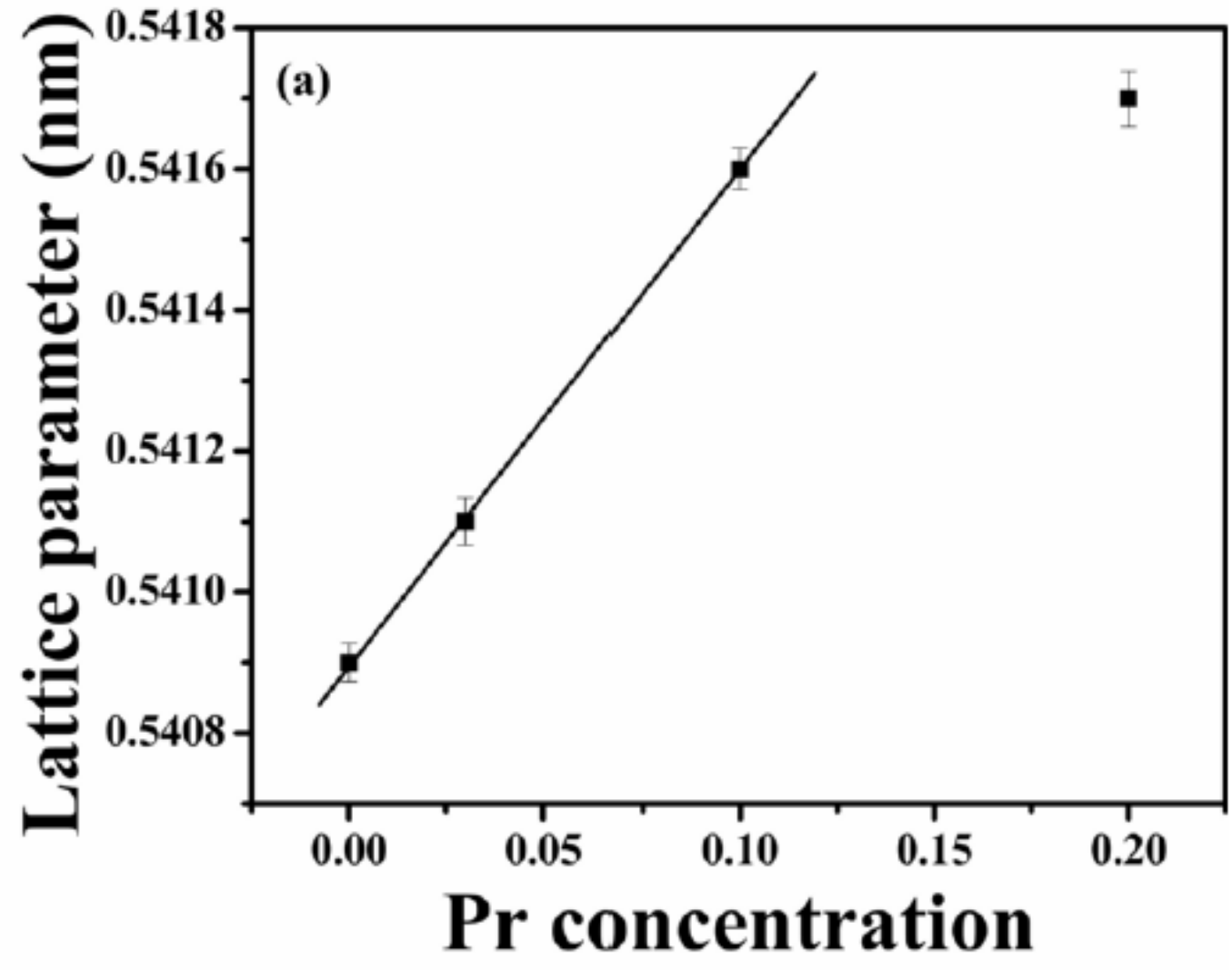
(a)
Lattice parameter (nm)
0.5418
0.5416
0.5414
0.5412
0.5410
0.5408
0.00
0.05
0.10
0.15
0.20
Pr concentration

FIG 7B

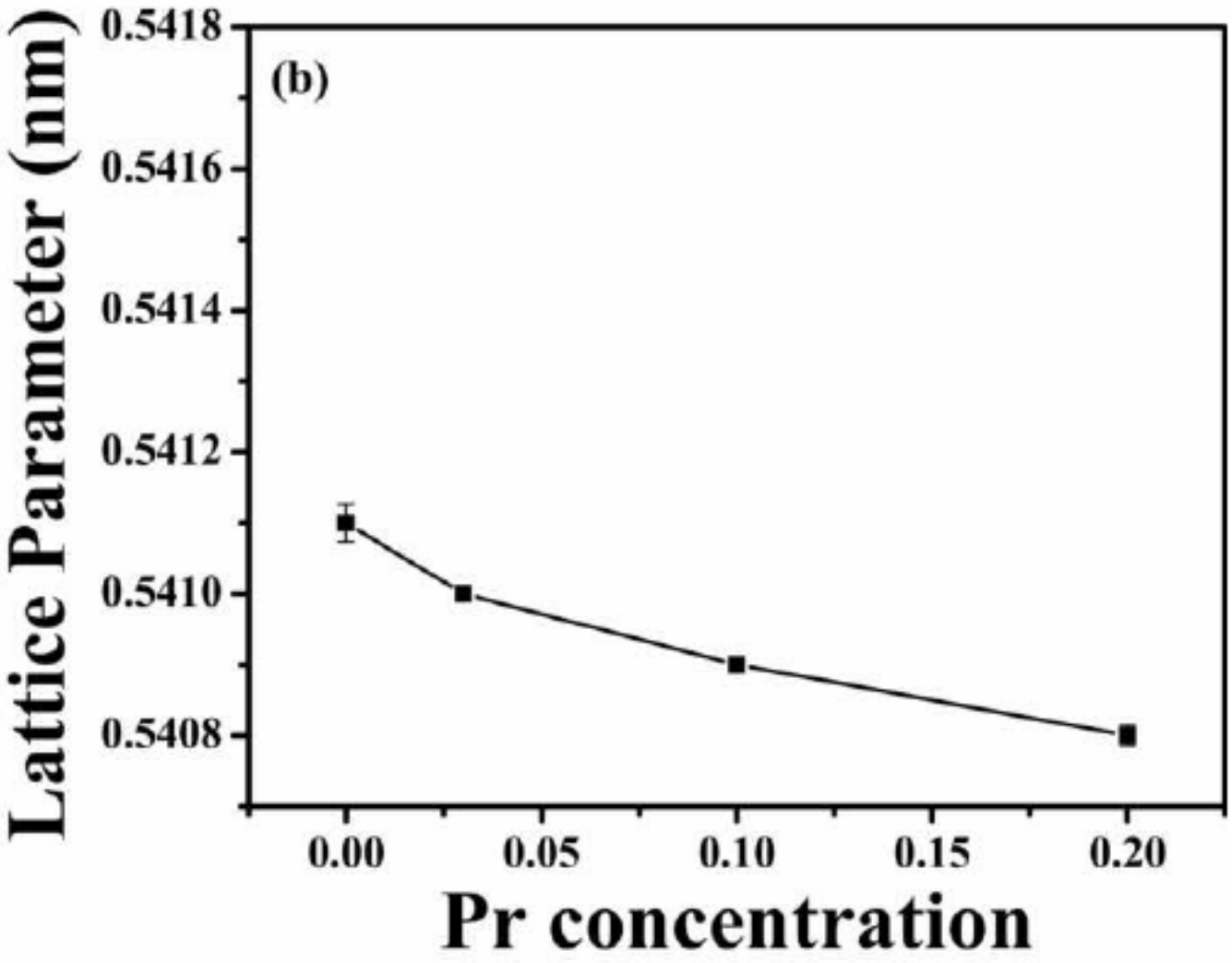
(b)
Lattice Parameter (nm)
0.5418
0.5416
0.5414
0.5412
0.5410
0.5408
0.00
0.05
0.10
0.15
0.20
Pr concentration